New Journal of Physics
The open-access journal for physics

The stability of vicinal surfaces and the equilibrium crystal shape of Pb by first principles theory

D K Yu[1], H P Bonzel[2] and M Scheffler[1]

[1] Theory Department, Fritz-Haber-Institut der Max-Planck-Gesellschaft, Faradayweg 4-6, 14195 Berlin, Germany
[2] Institut für Schichten und Grenzflächen, ISG-3, Forschungszentrum Jülich, 52425 Jülich, Germany
E-mail: h.bonzel@fz-juelich.de

New Journal of Physics **8** (2006) 65
Received 13 January 2006
Published 2 May 2006
Online at http://www.njp.org/
doi:10.1088/1367-2630/8/5/065

Abstract. The orientation-dependent surface energies of fcc Pb for more than 30 vicinal orientations, distributed over the [110] and [001] zones of the stereographic triangle, have been studied by density-functional theory. For bulk-truncated structures almost all vicinal surfaces are found to be unstable and would facet into (111) and (100) orientations. However, after surface relaxation, all vicinal surfaces are stable relative to faceting into (111) and (100) orientations. There are also regions of relaxed vicinal surfaces which will facet into nearby stable vicinal surfaces. Overall, surface relaxation significantly affects the equilibrium crystal shape (ECS) of Pb. In both the [110] and [001] crystallographic zones the (110), (112), (221), and (023) facets are found on the ECS only after relaxation, in addition to (111) and (100). This result is in agreement with the experimental ECS of Pb at 353 K. Step formation energies for various vicinal orientations are estimated from facet diameters of the theoretical ECS and compared with experimental data.

One of the fundamental problems of surface thermodynamics is to determine the shape of a crystal in thermodynamic equilibrium, where the total surface free energy is at an absolute minimum at constant volume and a certain temperature [1]. An early solution to this problem was given by Wulff a century ago [2], which stated that the equilibrium crystal shape (ECS) is the inner envelope of the perpendiculars to all radial vectors constructed from a polar plot of the anisotropic surface (free) energy (ASE). The knowledge of the complete ASE function is then a necessary condition for the construction of the ECS. Hence the computation of the complete surface energy anisotropy is highly desirable. From there it is straightforward to obtain the ECS.

PII: S1367-2630(06)16415-0

Early semi-quantitative attempts to generate information on the ASE of crystals were based on the simple method of counting broken surface bonds [3]. The lower the number of broken bonds in forming a surface, the lower the surface energy. For cubic crystals, this procedure already gives useful information on the relative ASE, in that minima were found at low-index (111), (100) and (110) orientations [4]. In the framework of thermodynamics, the stability of facets (phases) was studied as a function of temperature for bcc and fcc crystals [5]. Again, only low-index facets played a major role in this work. With the advent of surface structure calculations, based on empirical interaction potentials, it became possible to compute absolute values of surface energies for a number of materials, especially metals [6]. Soon first-principle techniques, in particular density-functional theory (DFT) [7], also provided absolute ASE data [8]–[14], but at first only for low-index surfaces. In addition, the complete ASE of metals, such as Ag, Cu, Rh and others was calculated by using empirical interaction potentials [15]–[18]. Frenken and Stoltze [16], applying effective medium theory to Ag, found the surprising result that all vicinal surfaces are unstable at $T = 0$ K. However, this result was questioned by Desjonquères *et al* [17] and it became obvious that calculations, which accounted for only first and second nearest-neighbour interactions, were of insufficient accuracy to supply a realistic ASE. They pointed out [17, 19] that higher order interactions have to be included or, even better, that electronic structure calculations are needed to obtain a reliable description of the ASE of metals.

The surface energy differences between different orientations are usually small. Comparing tight-binding and DFT calculations yields rather different results [17]. In the present work, we have employed DFT [20] together with the norm-conserving pseudopotential plane-wave method, to study the orientation-dependent surface energy of Pb. The technical details and results for low-energy surfaces have been reported elsewhere [21, 22]. Care has been taken to guarantee good numerical convergence. We use a plane-wave cut-off of 14 Ryd, Monkhorst–Pack **k** meshes equivalent or close to 24×24 for a Pb(100) surface, and slab of 12 (111) layers in the terrace for the (111) vicinals, 14 (100) layers in the terrace for the (100) vicinals and 18 (110) layers in the terrace for the (110) vicinals. The surface structures are fully relaxed, with a maximum force of less than 10 meV Å^{-1}. The average forces are one order of magnitude smaller. Surface energies will be reported in energy per unit area. The error bar for the surface energies relative to each other is estimated to be at the level of ± 0.05 meV Å^{-2} [22]. For the exchange-correlation functional, we used the local-density approximation (LDA) because the generalized gradient approximation (GGA) yields typically surface energies 30% lower than recent experimental values [21]. The good agreement with experiment is probably due to a better error cancellation of the surface exchange and correlation energy within the LDA [23, 24]. There is also excellent agreement between the calculated surface relaxations of Pb(111), (100) and (110) [21] and corresponding experimental data [25, 26].

Lead was chosen because extensive experimental work on the ECS of Pb crystallites had been carried out in the past [27]–[38]. Recently, high-resolution scanning electron tunnelling microscopy of Pb crystallites equilibrated at $T = 323$ K have shown large circular (100) facets, threefold symmetric (111) facets and additional twofold symmetric (112) and (221) facets in great detail [36]. Quantitative evaluations yielded absolute step free energies, step–step interaction energies, surface free energies and the complete ASE over the main [011] and [001] crystallographic zones. These experimental results provide an excellent base for a detailed comparison with theory, which was partially already reported elsewhere [21, 22]. In this paper we concentrate on the ASE, the stability of vicinal surfaces and the ECS of Pb at $T = 0$ K. The theoretical ECS will be compared with experimental images of the ECS of Pb recorded at

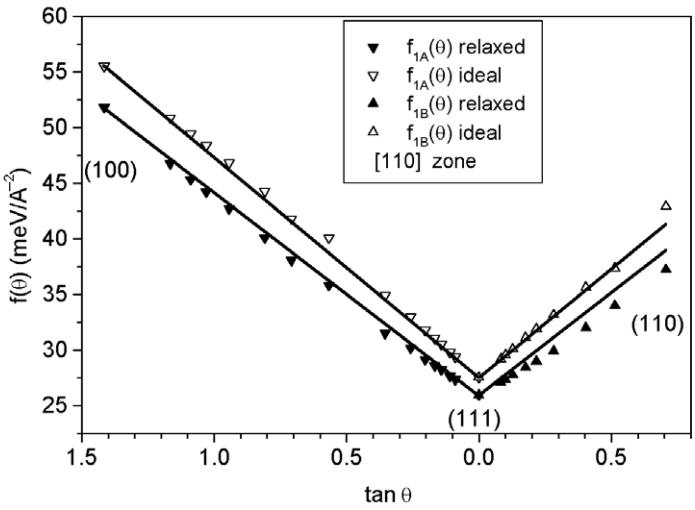

Figure 1. Plot of $f(\theta)$ versus $\tan\theta$ for unrelaxed and relaxed Pb surfaces in the $[01\bar{1}]$ and $[\bar{1}10]$ zones. Lines connecting (111) and (100) orientations of the same $[01\bar{1}]$ zone as well as connecting equivalent (111) orientations in the $[\bar{1}10]$ zone are drawn.

$T = 320$–353 K. No comparison can be made with experimental stability studies of Pb vicinal surfaces because they do not exist to our knowledge. A quantitative comparison of theoretical and experimental step energies will also be presented. Finally, we will compare step energies estimated from the theoretical ECS with corresponding values derived from the same theoretical ASE data using the thermodynamic definition of the ASE, $\gamma(\theta)$, which relates the first derivative of $\gamma(\theta)$ with respect to orientation θ, extrapolated to the limit of vanishing step density, to the step formation energy [22, 39].

The results of our DFT calculations of the ASE of Pb are summarized in figures 1 and 2 as plots of the projected surface energy, $f(\theta) = \gamma(\theta)/\cos\theta$, versus $\tan\theta$, where θ is the angle of misorientation relative to the nearest low-index (111) or (100) surfaces. Results are shown for the two major [110] and [001] zones encompassing the low-index orientations (111), (100) and (110). Two different data sets, one for unrelaxed surfaces and the other for fully relaxed surfaces, are presented. There are noteworthy differences between these two sets: firstly, the absolute values of surface energies are substantially higher for the unrelaxed surfaces, and secondly, because of the orientation-dependent surface relaxation energies, the degree of anisotropy is lower for the relaxed surfaces [15]. The primary calculated $\gamma(\theta)$ plots exhibit pronounced minima at the (111) and (100) orientations, so-called cusps, as well as a semi-cusp for the (110) orientation [22]. The data of figures 1 and 2 serve as the base for deriving information on the stability of vicinal Pb surfaces and for constructing the ECS of Pb crystallites.

To begin with the stability of vicinal surfaces, we refer to Herring's criterion for faceting of a surface of an arbitrary orientation defined by its normal $\mathbf{n}$ and area S, illustrated in figure 3, into stable facet orientations $\mathbf{n}_1$ with area S_1 and $\mathbf{n}_2$ with area S_2, respectively [40]:

$$\gamma(\mathbf{n})S > \gamma(\mathbf{n}_1)S_1 + \gamma(\mathbf{n}_2)S_2. \tag{1}$$

Usually at least one of the facet orientations is a low-index (low surface energy) orientation. The condition (1) which is a simple energy imbalance was shown to be equivalent to the following

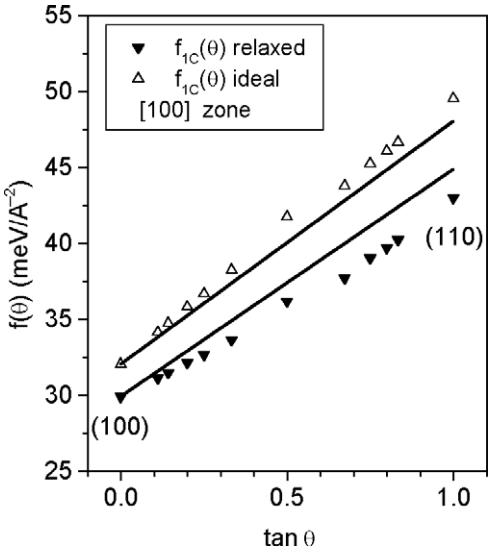

Figure 2. Plot of $f(\theta)$ versus $\tan\theta$ for unrelaxed and relaxed surfaces in the [001] zone. Lines connecting equivalent (100) orientations in the [001] zone are drawn.

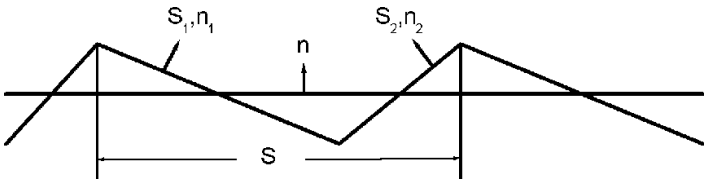

Figure 3. Schematic illustrating the faceting of a surface S with normal $\mathbf{n}$ into facets S_1 and S_2, with normals $\mathbf{n}_1$ and $\mathbf{n}_2$, respectively [17].

condition [16]

$$\Delta f(\theta) = f(\theta) - f_\ell(\theta) = f(\theta) - f(\theta_1) - \frac{f(\theta_2) - f(\theta_1)}{\tan\theta_2 - \tan\theta_1}(\tan\theta - \tan\theta_1) > 0, \tag{2}$$

where θ is a polar angle of orientation relative to a reference plane. Equation (2) means that a point on a straight line, $f_\ell(\theta)$, connecting the surface energies of stable low-index orientations, has to be subtracted from $f(\theta)$, and if $\Delta f(\theta) > 0$, faceting will occur. Alternatively, if $\Delta f(\theta) < 0$, the orientation is stable. Wanting to judge the stability of all orientations in figures 1 and 2, we make use of equation (2) and draw lines of $f_\ell(\theta)$ connecting a (111) and a (100) orientation or two equivalent (111) orientations in the [110] zone (figure 1). For the [001] zone, two equivalent (100) orientations are connected (figure 2). The lines are included in figures 1 and 2. Immediately, we recognize that nearly all surface orientations in their unrelaxed configuration are unstable while the relaxed surfaces are stable. This can be seen in more detail in the following figures 4 and 5 which show the energy differences $\Delta f(\theta)$ versus $\tan\theta$.

Figure 4 demonstrates that all orientations except (551) are unstable for the unrelaxed surfaces. For all relaxed surface orientations $\Delta f(\theta) < 0$, i.e. they will not facet into (111) and (100) orientations. However, there are local regions of instability, defined by inflection points, where the curvature changes from positive to negative. For example, the (113) and probably

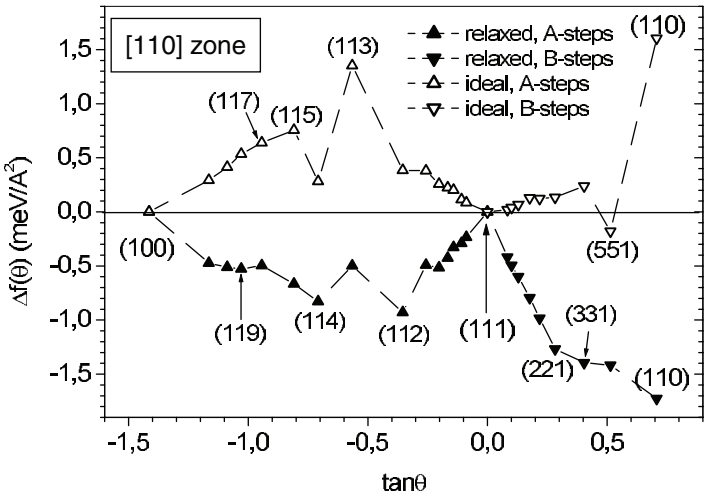

Figure 4. Plot of $\Delta f(\theta)$ versus $\tan\theta$ for unrelaxed and relaxed Pb surfaces in the $[01\bar{1}]$ and $[\bar{1}10]$ zones.

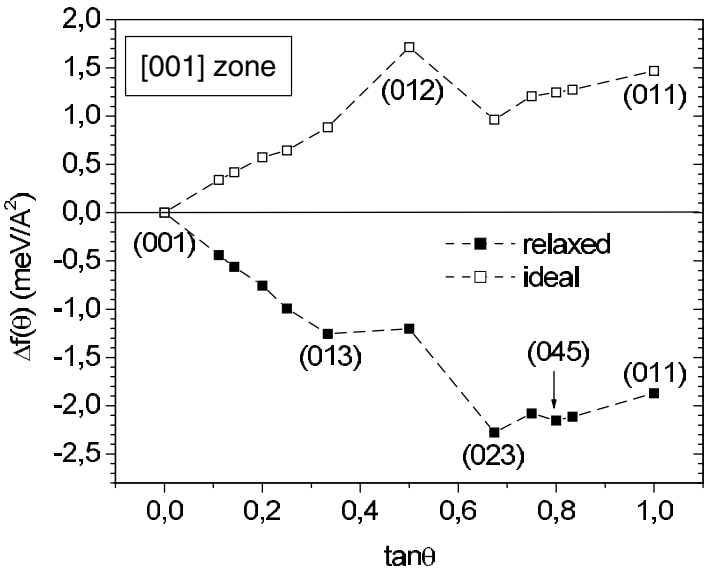

Figure 5. Plot of $\Delta f(\theta)$ versus $\tan\theta$ for unrelaxed and relaxed Pb surfaces in the [001] zone.

all neighbouring surfaces will facet into stable (114) and (112). A second region of instability is between (331), or perhaps (221), and (110). Orientations such as (115) and (117) are also unstable and will facet into (119) and (114) which suggest a broad region of instability. The surfaces of low energies and thus special stability are (110), (221), (112) and (114) in the [110] zone. The (114) is a special case because it exhibits two different steps per unit cell, with unequal step height and step separation. The same is true for the (551) surface. Vicinal surfaces of this kind appear to have relatively lower surface energy and thus higher stability than those with a single type of step.

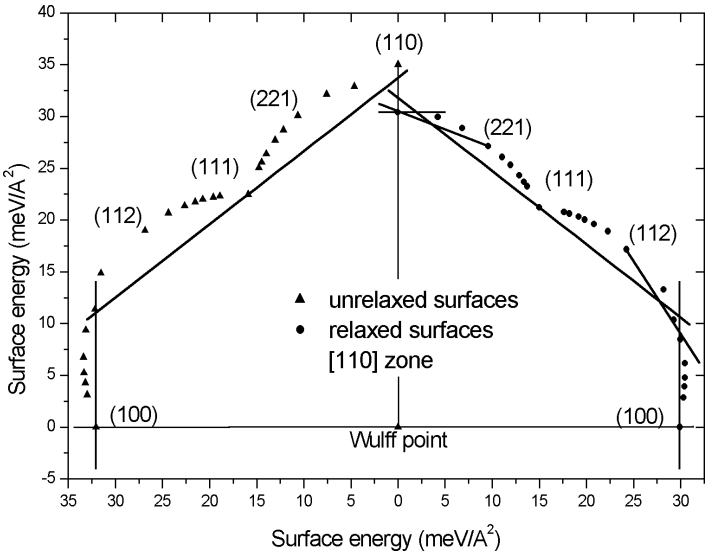

Figure 6. Single quadrants of a polar plot of $\gamma(\theta)$ and the constructed ECS for unrelaxed (on the left) and facets, new (112) and (221) facets are present on the relaxed crystal. A small (110) facet may also be present on the relaxed crystal. Sharp edges between facets are tentative because of a finite number of surface energy points.

The analogous situation for the [001] zone is illustrated in figure 5. Again the relaxed surfaces are stable with respect to faceting into (100) surfaces. The surface with the lowest $\Delta f(\theta)$ value and hence the highest relative stability is (023). There is a local region of instability around the (012) orientations; surfaces of lower θ in this region will facet into adjacent (013) and (023) orientations. A narrow region of instability is found at larger θ between (023) and (045). All orientations within this region should facet into the bounding stable orientations. Of course, it would be interesting to check some of these predictions experimentally.

Now we turn to the construction of parts of the ECS by using the theoretical surface energies of Pb in figure 1. Instead of constructing a three-dimensional ECS, it suffices to take a look at a cut of the ECS in a high symmetry [110] zone. There are two mirror planes in this zone, such that a single quadrant contains all relevant information on the anisotropy of $\gamma(\theta)$. Figure 6 shows a polar plot of the surface energy $\gamma(\theta)$ ('γ-plot') for a quadrant between (110) and (100) for the unrelaxed (left-hand side) and the relaxed (right-hand side) surfaces, respectively. Applying the Wulff construction point-by-point to $\gamma(\theta)$ [2], stable crystal facets are obtained. Facets are indicated by straight lines which are shown only for those $\gamma(\theta)$ points which actually define the ECS. Since $\gamma(\theta)$ is given by a finite number of data points, there is an uncertainty about the complete ECS, in particular concerning the transitions between neighbouring facets. These transitions may be continuous or discontinuous, in the latter case characterized by sharp edges separating facets. This uncertainty can unfortunately not be resolved on the basis of the computed digital $\gamma(\theta)$ function. We will return to this point further below.

Figure 6 shows remarkable differences between the ECS for the unrelaxed and relaxed surfaces which are consistent with the changes of surface stability due to relaxation. For unrelaxed surfaces, the only stable facets are (111) and (100) in this zone while the ECS for relaxed surfaces exhibits in addition (221) and (112) facets as well as evidence for a very small (110) facet. Stable

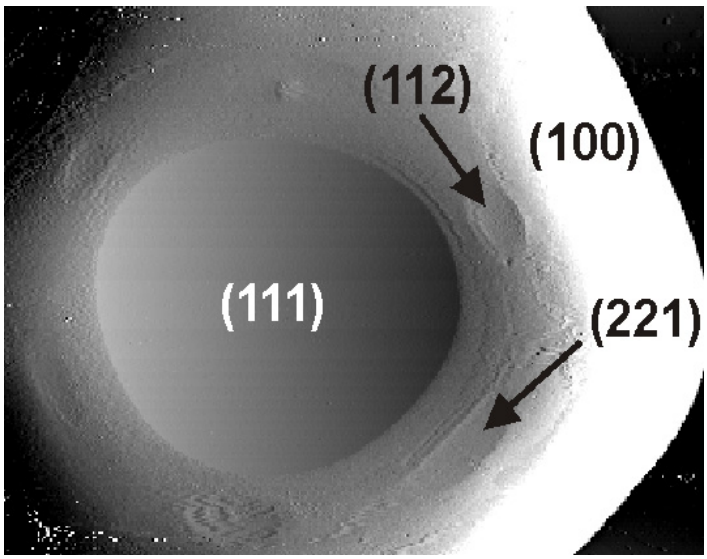

Figure 7. STM image of a portion of an equilibrated Pb crystallite [36]. Six twofold symmetric facets of (221) and (112) orientations are seen around the central (111) facet. A (100) facet is also present on the periphery of the truncated Pb crystallite whose diameter at the base is about 550 nm. The crystallite was equilibrated at $T = 353$ K.

(221) and (112) facets, located in the [110] zone, have indeed been found experimentally on the ECS around 300–353 K [36, 41] and on growth forms at $T = 323$ K [28]. The very small (110) facet in figure 6 has not been observed experimentally on the ECS. An example of a scanning electron tunnelling microscope (STM) image showing a (111) facet and neighbouring (211) and (112) facets is presented in figure 7 [36]. The crystallite was equilibrated at $T = 353$ K. The (112) facets can typically be observed at $T < 393$ K, while (221) facets have a lower range of existence at $T < 373$ K. Since the (111) plane of equilibrated Pb crystallites is parallel to the substrate surface and the (221) and (112) facets are less than 20° away from this plane, they are easily imaged by the STM. Facets further away on the round parts of the crystallite, especially if they are small or highly anisotropic, are much more difficult to detect. This is true for all possible facets in the [001] zone, for example, except the large round (100) facet which is located on the contact edge of the crystallite in figure 7.

Figure 8 shows the $\gamma(\theta)$-plot of surface energies in the [001] zone and the corresponding ECS. A quadrant is drawn for the unrelaxed and the relaxed surfaces. Again, relaxation causes a new orientation to be stable on the ECS, here the (023). The size of the (110) facet is large in this zone, almost the same diameter as that of the (100) facet. However, both are more than 35° away from the central (111) facet and thus have not been verified in the experimental STM images. Both (023) and (110) are twofold symmetric which further aggravates their detection. In fact, there is a large asymmetry in the (110) facet for the two perpendicular directions $[\bar{1}10]$ and [001] which is not surprising in view of the channel-like structure of this surface. The (110) cusp is deep in the [001] zone but very shallow in the $[\bar{1}10]$ zone ('knife-edge' cusp). This special feature is even supported by experimental surface free energy data at T = 473 K which show a cusp in [001] but not the $\bar{1}10]$ zone [27]. However, a clear twofold symmetric (110) facet of Pb

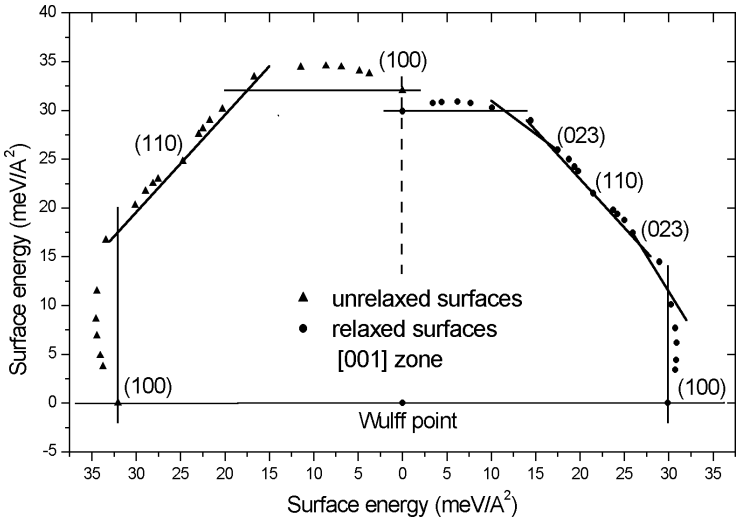

Figure 8. Single quadrants of a polar plot of $\gamma(\theta)$ and the constructed ECS for unrelaxed (on the left) and relaxed (on the right) surface energy data in the [001] zone. While the unrelaxed crystal shows only (110) and (100) facets, new (023) facets are present on the relaxed crystal. The sharp edges between facets are probably not realistic (see text).

with high aspect ratio has not been identified in an experimental ECS [36] although a (110) facet has been claimed to be present on the *growth* shape of a Pb crystallite [28].

The appearance of new facets due to surface relaxation may be typical for Pb because it is known to exhibit particularly large relaxations [13, 21, 25, 26, 42, 43]. The relaxation itself is of electronic origin, due to charge smoothing at the surface [44] and Friedel oscillations of the electron density near a surface which cause an electrostatic force to the ionic cores in the outermost layers. The significant decrease in surface energy due to relaxation, e.g. 5.6% for (111), 10% for (112) and (221), and 13.6% for (110) [22], changes the degree of surface energy anisotropy which then enables, for example, (023), (112) and (221) orientations to be stabilized and to appear on the relaxed ECS. In noble and transition metals, surface relaxations and related decreases in the surface energy are smaller than for Pb [14, 45]. Hence the effect on the ECS of those metals may not be so significant.

The radius of a facet on the ECS (in a high symmetry direction) is a measure of the energy of the step bounding the facet, provided the transition from facet to vicinal surface is continuous [39]. However, when the transitions between facets on the ECS at 0 K are discontinuous, such as tentatively drawn in figures 6 and 8, it is still possible to obtain a *lower* limit for the step energies from the facet radii [46, 47]. On the other hand, if the transitions were actually continuous, the values determined from the facet radii, such as drawn in figures 6 and 8, would be an *upper* limit of the step energies. At this point, we note that step energies of Pb have been determined from the same ASE data according to the thermodynamic definition mentioned above [39] which requires a linear dependence of $f(\theta)$ versus $\tan\theta$ in a region close to a low-index facet orientation [22]. Such a dependence was proven to exist for Pb surfaces vicinal to (111), (100) and (110) surfaces. Corresponding step energies have been evaluated and reported [22].

From the foregoing it is now of interest to estimate step energy values from the facets in figures 6 and 8 and to compare them with those obtained via the thermodynamic definition of

Table 1. Comparison of step energies for relaxed surfaces of Pb, derived from the ECS facet radii (figures 6 and 8), from the thermodynamic definition of anisotropic $f(\theta)$ versus $\tan\theta$ in the limit of $\theta \to 0$ [22, 39], and obtained experimentally [36, 48]. The step direction is identical to the crystallographic zone axis.

Facet/Zone/Step type[a]	r_f/z_0	Step energy $f_1(0)$ derived from ECS (meV Å^{-2})	Step energy $f_1(0)$ according to thermodynamic definition [22] (meV Å^{-2})	Step energy $f_1(T)$ from experiment [36, 48] (meV Å^{-2})
(111)/[110]/A	0.599	$\geqslant$15.6	15.8	12.8[b]
(111)/[110]/B	0.533	$\geqslant$13.8	13.9	11.6[b]
(100)/[110]/A	0.303	$\geqslant$9.1	8.9	8.1[c]
(100)/[001]/C	0.390	$\geqslant$11.4	11.2	–
(110)/[110]/B	0.009	$\approx$0.3	–	–
(110)/[001]/C	0.248	$\geqslant$7.5	5.9	–
(221)/[110]	0.066	$\geqslant$1.9	–	1.3[c]
(112)/[110]	0.062	$\geqslant$1.8	–	1.0[c]
(023)/[001]	0.087	$\geqslant$2.7	–	–

[a]Steps A and B vicinal to (111)[110] are inequivalent because of the threefold symmetry of the (111) surface. Steps A, B and C are distinguished by their edge structures, namely (100), (111) and (110), respectively.
[b]$T = 0$ K.
[c]$T = 323$ K.

the step energy [22]. For this reason we measure graphically the ratio of the facet radius, r_f, over the facet separation from the crystal centre, z_0, for each facet to obtain the step energy $f_1(0)$ of the corresponding vicinal surface. The relationship is simply $f_1^i(0) = [r_{fi}(0)/z_{0i}(0)]f_{0i}(0)$, where $f_{0i}(0)$ is the surface energy of facet 'i'. For the (111) and (100) facets the inequivalent step energies of the relaxed surfaces are $f_{1A}^{111}(0) \geq 15.5$ meV Å^{-2}, $f_{1B}^{111}(0) \geq 13.9$ meV Å^{-2}, $f_{1A}^{100}(0) \geq 9.1$ meV Å^{-2} and $f_{1C}^{100}(0) \geq 11.4$ meV Å^{-2}. These estimates are quite close to the values obtained previously using the thermodynamic derivation [22], compare table 1. For the unrelaxed crystal the corresponding values are, for example, $f_{1A}^{111}(0) \geq 19.6$ meV Å^{-2} and $f_{1A}^{100}(0) \geq 11.0$ meV Å^{-2} which are also consistent with the thermodynamic evaluation. The step energies for the (112) and (221) orientations in the [110] zone are estimated as $f_1^{211}(0) \geq 1.8$ meV Å^{-2} and $f_1^{211}(0) \geq 1.9$ meV Å^{-2}. The ratio of step energies for vicinal Pb(111) in the relaxed configuration is determined from the ECS as $f_{1B}(0)/f_{1A}(0)$=0.88 which is in good agreement with the experimental ratio of 0.91. Likewise, the energies of the steps bounding the (110) facet can be estimated as $f_{1B}^{110}(0) \geq 0.3$ meV Å^{-2} and $f_1^{221}(0) \geq 1.9$ meV Å^{-2}, respectively, suggesting an aspect ratio of 25. In the latter case the value of the step energy (110)[001]C estimated from the ECS is considerably *larger* than the value determined thermodynamically. A similar but much less significant discrepancy is noted for the (100) step energies (see table 1).

The overall comparison in table 1 shows that the step energies of vicinal surfaces estimated from the ECS are almost the same (except for (110)[001]/C) as those derived via

the thermodynamic definition [22]. In other words, the lower limit meets the true value of the step energy. This result suggests strongly that the transitions between facets and vicinal surfaces for the calculated ECS of Pb (at $T = 0$ K) are continuous, i.e. that there should be rounded edges between neighbouring facets. This can be proven if a much higher density of surface energy points were calculated to provide a quasi-continuous $\gamma(\theta)$ function. The transition region may in fact be very narrow on the ECS. In the case of the (110)[001] C-step the lower limit surpasses the thermodynamic value of the step energy by 1.6 meV Å^{-2} which is a clear indication that the transition between (110) and (023) facets must be continuous, or alternatively, that other facets may exist in this transition region. Hence the estimates for both (110) and (023) vicinal step energies in this zone, based on facet radii, are not trustworthy. Finally, we note that the theoretical ratio of C/A step energies for the (100) facet in table 1 is about 1.26. Hence the facet is not a square at $T = 0$ K but probably an irregular octagon. At $T > 0$ it may turn into a square with round corners. The reason for a C/A ratio $<\sqrt{2}$ may be due to next nearest-neighbour interactions and zero point vibrational energy [49]. The theoretical C/A ratio for Pb is thus remarkably close to an experimental ratio of 1.24 (extrapolated to $T = 0$ K) determined for equilibrated Cu(100) islands [50].

We also list experimental values for step free energies [36] in table 1 and note that there is reasonable agreement with the step energies obtained theoretically. For the (111) vicinal steps the experimental values are determined and quoted at $T = 0$ K [48]. The 13–16% difference can be due to experimental error and has been discussed elsewhere [22]. The other values are obtained at $T = 323$ K by scaling to experimental surface free energies of the corresponding facet orientations [36]. The higher temperature causes the step free energies to be lower than at $T = 0$ K. At this point we discuss briefly the temperature dependence of the ECS which is closely related to the temperature dependence of facet shapes and sizes. The latter is directly related to the step free energies [39] whose temperature dependence is governed by mainly two effects: firstly, the thermal excitation of kinks and the associated meandering of steps, and secondly, higher amplitudes of vibrations of step and kink atoms compared to terrace atoms [51, 52], giving rise to a vibrational entropy term [16, 53]. Both effects have been accounted for by thermodynamic theory where the vibrational entropy has been estimated [54, 55] as well as calculated in the framework of lattice dynamical models of increasing complexity [52, 56]. The dominant effect, especially at elevated temperatures, is thermal kink formation which leads to terms that depended exponentially on temperature in the expression for the step free energy, $f_1(T)$. The lower the kink energy, the stronger the decrease in $f_1(T)$. For facets with inequivalent step energies there can be different kink energies as well, so for the (111) facet [48]. For the fourfold symmetric (100) facet there are two different step energies but only one kink energy for the [110] step because the [100] step is already fully kinked at $T = 0$ K. The shape change of the facet can be described by Ising theory [50] or by including first and second neighbour interactions at the step edge as well as a vibrational energy term [49]. The expected octagonal shape near 0 K (with rounded corners) changes into a circular shape at high temperature. Twofold symmetric facets, such as (110), (211) and (221), are also bound by two inequivalent steps, one of which is fully kinked. With increasing temperature the aspect ratios of the oval facets decrease due to kink formation on the close-packed step and vibrational entropy. High temperature leads eventually to the disappearance of each facet except Pb(111). The temperature of disappearance is characteristic of the facet orientation and thus indicative of a roughening transition of this facet. At the roughening temperature the free energies of the steps bounding the facet become zero. In other words, as long as a facet is visible, e.g. the (211) facet at 353 K in figure 7, the

corresponding surface has not undergone a roughening transition. Even more, these surfaces are well below their surface melting temperature [57, 58], provided such a transition exists for a particular surface.

The vibrational entropy is equally important for the temperature dependence of the step free energy. In the harmonic regime it is a constant quantity at low temperatures but may be increasing at high temperature because of anharmonicity. The latter is expected for Pb since evidence for anharmonic surface vibrations has been detected for Pb(110) at $T > 400$ K [59]. The order of magnitude of the vibrational step entropy in the harmonic approximation has been estimated as 0.03–0.05 meV K^{-1} per atom for close-packed steps on vicinal (111) surfaces of Pb and Ag [16, 53]. Returning to table 1 we note a decrease in the step free energies from 0 to 323 K for the (100)[110]A, the (221)[110] and (211)[110] steps of 10 to over 40%. The (100) facet exhibits the lower relative decrease of about 0.9 meV $Å^{-2}$ and has a circular shape at 323 K, i.e., only one step free energy is quoted. The step entropy for this type of step is estimated as 0.017 meV K^{-1} per atom. At 323 K the step vibrational free energy amounts then to about -0.6 meV $Å^{-2}$ which accounts for more than half of the decrease at 323 K while the rest has to be attributed to the meandering entropy of the step. For the (221) and (211) steps the decrease in $f_1(T)$ at 323 K is also expected to be due to vibrational entropy and kink formation because both orientations are not far from their roughening temperature at $T < 393$ K. In this case, we will not attempt to decompose the observed decrease in $f_1(T)$ of 0.6–0.8 meV $Å^{-2}$ into vibrational and meandering free energy contributions. Overall, the experimental step-free energies are qualitatively consistent with the theoretical results in table 1.

In summary, an extensive set of theoretical surface energy data of Pb obtained by DFT calculations enables us to provide detailed information on the stability of vicinal surfaces in the [110] and [001] zones of Pb. A major result is that surface relaxation has a profound influence on the stability of vicinal surfaces at $T = 0$ K. The ECSs of unrelaxed and relaxed Pb were also determined in the same zones. For unrelaxed surfaces the only facets are (111) and (100) in the [110] zone. Relaxation causes, in addition, highly anisotropic (110), (112), (221) and (023) facets to appear. Step energies of surfaces vicinal to these facets have been estimated from the facet radii and compared with data derived previously by a continuum thermodynamics approach. The close agreement suggests that there are probably no sharp edges on the ECS of Pb at $T = 0$ K. A comparison of theoretical and experimental step energies shows reasonable agreement when the effect of temperature is considered.

Acknowledgments

We thank George Comsa and Marek Nowicki for their careful reading of this paper and numerous suggestions for improvements.

References

[1] Herring C 1951 *Phys. Rev.* **82** 87
[2] Wulff G 1901 *Z. Kristallogr.* **34** 449
[3] MacKenzie J K, Moore A J W and Nicholas J F 1962 *J. Phys. Chem. Solids* **23** 185
[4] Nicholas J F 1968 *Aust. J. Phys.* **21** 21

[5] Rottman C and Wortis M 1984 *Phys. Rev.* B **29** 328
[6] Foiles S M, Baskes M I and Daw M S 1986 *Phys. Rev.* B **33** 7983
[7] Kohn W and Sham L J 1965 *Phys. Rev.* A **140** 1133
[8] Mansfield M and Needs R J 1991 *Phys. Rev.* B **43** 8829
[9] Methfessel M, Henning D and Scheffler M 1992 *Phys. Rev.* B **46** 4816
[10] Methfessel M, Henning D and Scheffler M 1992 *Appl. Phys.* A **55** 442
[11] Stumpf R and Scheffler M 1994 *Phys. Rev. Lett.* **72** 254
[12] Vitos L, Ruban A V, Skriver H L and Kollár J 1998 *Surf. Sci.* **411** 186
[13] Feibelman P 2000 *Phys. Rev.* B **62** 17020
[14] Galanakis I, Bihlmayer G, Bellini V, Papanikolaou N, Zeller R, Blügel S and Dederichs P H 2002 *Europhys. Lett.* **58** 751–7.
[15] Wolf D 1990 *Surf. Sci.* **226** 389
[16] Frenken J W M and Stoltze P 1999 *Phys. Rev. Lett.* **82** 3500
[17] Desjonquères M C, Spanjaard D, Barreteau C and Raouafi F 2002 *Phys. Rev. Lett.* **88** 056104
[18] Wang X, Jia Y, Yao Q, Wang F, Ma J and Hu X 2004 *Surf. Sci.* **551** 179
[19] Raouafi F, Barreteau C, Spanjaard D and Desjonquères M C 2002 *Phys. Rev.* B **66** 045410
[20] Bockstedte M, Kley A, Neugebauer J and Scheffler M 1997 *Comput. Phys. Commun.* **107** 187
[21] Yu D and Scheffler M 2004 *Phys. Rev.* B **70** 155417
[22] Yu D, Bonzel H P and Scheffler M 2005 unpublished
[23] Perdew J P, Burke K and Ernzerhof M 1996 *Phys. Rev. Lett.* **77** 3865
[24] Staroverov V N, Scuseria G E, Tao J and Perdew J P 2004 *Phys. Rev.* B **69** 075102
[25] Frenken J W M, van der Veen J F, Barnett R N, Landman U and Cleveland C L 1986 *Surf. Sci.* **172** 319
[26] Li Y S, Quinn J, Jona F and Marcus P M 1989 *Phys. Rev.* B **40** 8239
[27] Heyraud J C and Métois J J 1983 *Surf. Sci.* **128** 334
[28] Heyraud J C and Métois J J 1987 *J. Cryst. Growth* **82** 269
[29] Heyraud J C, Métois J J and Bermond J M 1989 *J. Cryst. Growth* **98** 355
[30] Pavlovska A, Dobrev D and Bauer E 1995 *Surf. Sci.* **326** 101
[31] Pavlovska A, Faulian K and Bauer E 1989 *Surf. Sci.* **221** 233–43.
[32] Gangopadhyay U and Wynblatt P 1994 *Metall. Mater. Trans.* A **25** 607
[33] Arenhold K, Surnev S, Bonzel H P and Wynblatt P 1999 *Surf. Sci.* **424** 271
[34] Thürmer K, Reutt-Robey J E, Williams E D, Uwaha M, Emundts A and Bonzel H P 2001 *Phys. Rev. Lett.* **87** 186102
[35] Emundts A, Nowicki M and Bonzel H P 2002 *Surf. Sci.* L**496** 35–42.
[36] Bombis C, Emundts A, Nowicki M and Bonzel H P 2002 *Surf. Sci.* **511** 83
[37] Nowicki M, Bombis C, Emundts A, Bonzel H P and Wynblatt P 2002 *New J. Phys.* **4** 60
[38] Nowicki M, Emundts A and Bonzel H P 2003 *Prog. Surf. Sci.* **74** 123
[39] Wortis M 1988 *Chemistry and Physics of Solid Surfaces* vol 7, ed R Vanselow and R Howe (New York: Springer) pp 367–405
[40] Herring C 1952 The use of classical macroscopic concepts in surface energy problems *Structure and Properties of Solid Surfaces* ed R Gomer and C S Smith (Chicago, IL: University of Chicago Press) p 5
[41] Bonzel H P 2003 *Phys. Rep.* **385** 1–67.
[42] Lin R F, Li Y S, Jona F and Marcus P M 1990 *Phys. Rev.* B **42** 1150
[43] Li Y S, Jona F and Marcus P M 1991 *Phys. Rev.* B **43** 6337
[44] Smoluchowski R 1941 *Phys. Rev.* **60** 661
[45] Galanakis I, Papanikolaou N and Dederichs P H 2002 *Surf. Sci.* **511** 1–12
[46] Emundts A, Bonzel H P, Wynblatt P, Thürmer K, Reutt-Robey J and Williams E D 2001 *Surf. Sci.* **481** 13
[47] Mullins W W 2001 *Interface Sci.* **9** 9–20
[48] Nowicki M, Bombis C, Emundts A and Bonzel H P 2003 *Phys. Rev.* B **67** 075405
[49] van Moere R, Zandvliet H J W and Poelsema B 2003 *Phys. Rev.* B **67** 193407

[50] Giesen M, Steimer C and Ibach H 2001 *Surf. Sci.* **471** 80
[51] Durukanoglu S, Kara A and Rahman T S 2003 *Phys. Rev.* B **67** 235405
[52] Rahman T S, Kara A and Durukanoglu S 2003 *J. Phys.: Condens. Matter* **15** S3197
[53] Bonzel H P and Emundts A 2000 *Phys. Rev. Lett.* **84** 5804
[54] Zandvliet H J W, Gurlu O and Poelsema B 2001 *Phys. Rev.* B **64** 073402–1.
[55] Zandvliet H J W, van Moere R and Poelsema B 2003 *Phys. Rev.* B **68** 073404
[56] Tréglia G and Desjonquères M-C 1985 *J. Phys. (Paris)* **46** 987
[57] Frenken J W M and van der Veen J F 1985 *Phys. Rev. Lett.* **54** 134
[58] Pluis B, Denier van der Gon A W, Frenken J W M and van der Veen J F 1987 *Phys. Rev. Lett.* **59** 2678
[59] Frenken J W M, Huussen F and van der Veen J F 1987 *Phys. Rev. Lett.* **58** 401